

THE SIGNATURE OF A WIND REVERSE SHOCK IN GAMMA-RAY BURST AFTERGLOWS

ASAF PE'ER¹ AND RALPH A. M. J. WIJERS¹

Received 2005 November 16; accepted 2005 December 27

ABSTRACT

Explosions of massive stars are believed to be the source of a significant fraction of gamma-ray bursts (GRBs). If this is indeed the case, then the explosion blast wave propagates into a complex density structure, composed of a stellar wind bounded by two shock waves—a wind reverse shock and a forward shock. As the explosion blast wave reaches R_0 , the radius of the wind reverse shock, it splits into two shock waves—a reverse and a forward shock wave. We show that the reverse shock thus produced is not strong; therefore, full analytical treatment is required in calculating its properties. We calculate the dynamics of the flow and the evolution of the blast waves in all of the different stages. We show that the fluid Lorentz factor at $r > R_0$ is equal to 0.725 times the blast wave Lorentz factor as it reaches R_0 and is time (and r) independent as long as the blast wave reverse shock exists. Following the calculation of the blast wave evolution, we calculate the radiation expected in different energy bands. We show that about a day after the main explosion, as the blast wave reaches R_0 , the observed afterglow flux starts to rise. It rises by a factor of about 2 in a few hours, during which the blast wave reverse shock exists, and then declines. We show that the power-law index describing the light-curve time evolution is different at early (before the rise) and late times and is frequency dependent. We present light curves in the different energy bands for this scenario.

Subject headings: gamma rays: bursts — gamma rays: theory — plasmas — radiation mechanisms: nonthermal — shock waves

Online material: color figures

1. INTRODUCTION

In recent years, there is increasing evidence that long-duration ($t_{90} \geq 2$ s; Kouveliotou et al. 1993) GRBs are associated with the deaths of massive stars, presumably arising from core collapse (Woosley 1993; Levinson & Eichler 1993; MacFadyen & Woosley 1999; MacFadyen et al. 2001; Zhang et al. 2003). This evidence includes the association of some GRBs with Type Ib/c supernovae (GRB 980425 and SN 1998bw [Galama et al. 1998]; GRB 011121 and SN 2001ke [Garnavich et al. 2003]; GRB 030329 and SN 2003dh [Hjorth et al. 2003; Stanek et al. 2003]; and GRB 031203 and SN 2003lw [Malesani et al. 2004]), as well as the association of GRBs with massive star-forming regions in distant galaxies (Paczynski 1998; Wijers et al. 1998; Fruchter et al. 1999; Trentham et al. 2002). Further clues arise from evidence of high column densities toward GRBs, which associate GRBs with molecular clouds (e.g., Galama & Wijers 2001).

If indeed GRBs are associated with the deaths of massive stars, then the circumburst environment is influenced by the wind from the star. As supersonic wind from the star meets the interstellar medium (ISM), two shock waves are formed: a forward shock wave that propagates into the ISM, and a reverse shock that propagates into the wind (in the wind rest frame). The “wind bubble” thus formed is composed of the unshocked wind, the shocked wind, and the shocked ISM (Castor et al. 1975; Weaver et al. 1977). This complex structure of the circumburst environment is expected to affect the dynamics of the GRB blast wave during its late (afterglow) evolution and hence to have an observable effect on the afterglow emission (Wijers 2001; Ramirez-Ruiz et al. 2001, 2005; Chevalier et al. 2004; Eldridge et al. 2006).

The main effect is expected to take place when the relativistic blast wave reaches the density discontinuity produced by the

wind reverse shock. The blast wave then splits into two shock waves—a blast wave forward shock and a blast wave reverse shock (Sari & Piran 1995; Ramirez-Ruiz et al. 2005). The blast wave reverse shock thus produced propagates into a wind that was already shocked by the original blast wave prior to its split. This wind is hot; therefore, the ratio of the energy densities, or of the gas pressures downstream and upstream of the flow past the blast wave reverse shock, is not much greater than unity. Hence, the blast wave reverse shock is not strong. Obviously, as the blast wave splits into two, the dynamics of the created shock waves can no longer be described by a self-similar motion (Blandford & McKee 1976), which determines the evolution of the original relativistic blast wave at earlier stages, as well as the dynamics at a much later stage.

In this paper, we analyze in detail the effect of the circumburst environment on the dynamics of the blast wave(s). Following the analysis of Castor et al. (1975), we determine in § 2 expected circumburst conditions for a GRB progenitor. In § 3 we use the jump conditions at the blast wave reverse and forward shocks to show that a simple analytic relation between the velocity of the shocked fluid prior to the blast wave split and the velocity of the shocked fluid after the split is obtained. We further find a simple analytic relation that connects the Lorentz factor of the reverse shock to the Lorentz factor of the fluid as it reaches the contact discontinuity. We use these results to determine in § 4 the evolution of the fluid velocity. We calculate in § 5 the resulting light curves in different energy bands, before summarizing and discussing the implications of our findings in § 6.

2. THE CIRCUMBURST ENVIRONMENT

The circumburst environment during the GRB explosion depends on the evolutionary stages of the progenitor prior to its final (presumably, Wolf-Rayet) phase. A standard evolutionary track for a massive galactic star is to start as an O star, evolve through a red supergiant (RSG) or luminous blue variable phase,

¹ Astronomical Institute “Anton Pannekoek”, Kruislaan 403, 1098SJ Amsterdam, Netherlands; apeer@science.uva.nl.

before ending as a Wolf-Rayet star (García-Segura et al. 1996a, 1996b). The RSG phase may be absent for low-metallicity stars (Chieffi et al. 2003), which are preferred as GRB progenitors (Le Floc'h et al. 2003; Fynbo et al. 2003; Vreeswijk et al. 2004), or for rapidly rotating stars (Petrovic et al. 2005).

We thus consider a massive ($M \gtrsim 25 M_\odot$), low-metallicity ($Z \sim 0.01$) star as a GRB progenitor. During the Wolf-Rayet phase of the star, which lasts a duration of $\sim 10^6$ yr, the star loses mass at a typical mass-loss rate of $\dot{M} \approx 10^{-6} M_\odot \text{ yr}^{-1}$, producing a wind characterized by a typical velocity $v_w \sim 1000 \text{ km s}^{-1}$, presumably steady during most of the Wolf-Rayet phase of the star (Vink et al. 2000; Chevalier et al. 2004; Vink & de Koter 2005). The evolution of the wind-driven circumstellar shell was first derived by Castor et al. (1975) and Weaver et al. (1977). It was shown that during most of its lifetime (neglecting very short early stages), the system has four zones consisting, from the inside out, of (a) a hypersonic stellar wind with characteristic density $n_a(r) = \dot{M}/(4\pi m_p r^2 v_w)$; (b) a hot, almost isobaric region consisting of shocked stellar wind mixed with a small fraction of swept-up interstellar gas; (c) a thin, dense shell containing most of the swept-up interstellar gas; and (d) ambient interstellar gas.

Neglecting the width of region (c) compared to region (b) (see below), and assuming that most of the energy in region (b) is in the form of thermal energy, it was shown by Castor et al. (1975) that the outer termination shock radius is at

$$R_{\text{FS},w} = \left(\frac{125}{308\pi} \right)^{1/5} \left(\frac{\dot{M} v_w^2 t_*^3}{\rho_{\text{ISM}}} \right)^{1/5} \\ = 1.6 \times 10^{19} \dot{M}_{-6}^{1/5} v_{w,8}^{2/5} n_{0,3}^{-1/5} t_{*,6}^{3/5} \text{ cm}, \quad (1)$$

where $\dot{M} = 10^{-6} \dot{M}_{-6} M_\odot \text{ yr}^{-1}$, $v_w = 10^8 v_{w,8} \text{ cm s}^{-1}$, the ambient ISM density is $\rho_{\text{ISM}} = m_p n_{\text{ISM}}$, $n_{\text{ISM}} = 10^3 n_{0,3} \text{ cm}^{-3}$, and $t_* = 10^6 t_{*,6} \text{ yr}$ is the lifetime of the Wolf-Rayet phase of the star. Here we have scaled the ambient density to a value typical of a molecular cloud, in which we assume the young star to be still embedded. The density of the swept-up ISM matter in region (c) is approximated by its value for a strong, adiabatic shock, $\rho_c \simeq 4\rho_{\text{ISM}}$.² Comparison of the total ISM mass swept up to radius $R_{\text{FS},w}$, $M_{\text{ISM}} \simeq (4\pi/3) R_{\text{FS},w}^3 \rho_{\text{ISM}}$, to the mass in region (c), $\approx 4\pi R_{\text{FS},w}^2 \Delta R_c \rho_c$, then leads to the conclusion that the width of region (c) is $\Delta R_c \approx R_{\text{FS},w}/12$.

The pressure in regions (b) and (c) is $P_b = P_c = (2/3)u_b$ (assuming a monatomic gas), where u_b is the energy density in region (b), or

$$P_b = P_c = \frac{7}{25} \left(\frac{125}{308\pi} \right)^{2/5} \rho_{\text{ISM}} \left(\frac{\dot{M} v_w^2}{\rho_{\text{ISM}} t_*^2} \right)^{2/5} \\ = 1.4 \times 10^{-10} \dot{M}_{-6}^{2/5} v_{w,8}^{4/5} n_{0,3}^{3/5} t_{*,6}^{-4/5} \text{ dynes cm}^{-2}. \quad (2)$$

The radius of the inner (reverse) shock was calculated by Weaver et al. (1977; see also García-Segura & Franco 1996), assuming that the pressure in region (b) is much larger than the pressure in region (a), $P_b \gg P_a$ (strong shock assumption), by equating the momentum flux upstream and downstream of the shock. Com-

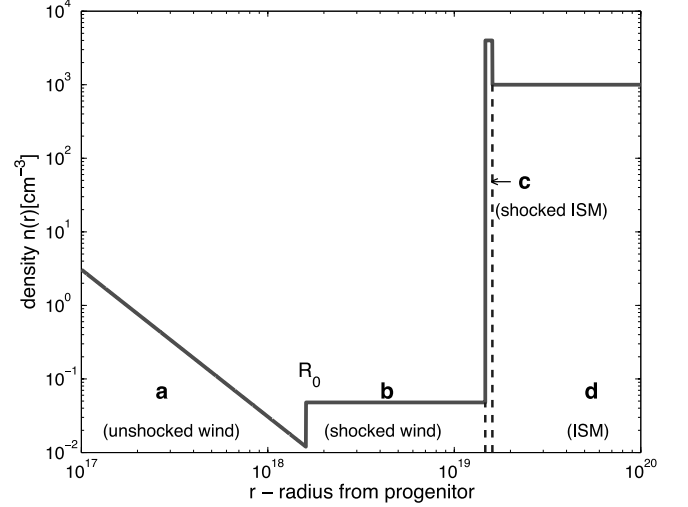


FIG. 1.—Schematic density profile for the scenario of a massive star emitting a wind. Region (a) consists of the unshocked wind, with a density profile $n(r) \propto r^{-2}$. Region (b) consists of a hot, nearly isobaric, shocked wind. Region (c) consists of the shocked ISM, and region (d) is the unshocked ISM. [See the electronic edition of the Journal for a color version of this figure.]

parison of the ram pressure in the upstream region (a), $\rho_a(R_0)v_w^2$, to the pressure downstream, $P_b + \rho_b v_b^2$, leads to

$$R_0 \equiv R_{\text{RS},w} = \left(\frac{3}{4} \frac{\dot{M} v_w}{4\pi P_b} \right)^{1/2} \\ = 1.6 \times 10^{18} \dot{M}_{-6}^{3/10} v_{w,8}^{1/10} n_{0,3}^{-3/10} t_{*,6}^{2/5} \text{ cm}, \quad (3)$$

where $\rho_a(R_0) = \dot{M}/(4\pi R_0^2 v_w)$, $\rho_b = 4\rho_a$, and $v_b = v_w/4$ (strong shock assumptions) were used. The number density of particles in region (a) is $n_a(r) \propto r^{-2}$ and at $r = R_0$ is given by

$$n_a(R_0) = \frac{\dot{M}}{4\pi m_p R_0^2 v_w} = 3.0 \times 10^{-2} R_{0,18}^{-2} \dot{M}_{-6} v_{w,8}^{-1} \text{ cm}^{-3}, \quad (4)$$

where $R_0 = 10^{18} R_{0,18} \text{ cm}$.³ The density in region (b) depends on the uncertain physics of the heat conduction. Heat conduction could be prevented by a magnetic field, which is expected to be toroidal in this region (Chevalier et al. 2004). Under this assumption, and using the fact that the internal speed of sound in this region is much higher than the expansion velocity, the number density in region (b) is approximately r -independent and is equal to $n_b \simeq 4n_a(R_0)$ (Weaver et al. 1977; see also Dyson & Williams 1997).

A schematic density profile of the bubble is shown in Figure 1. While being only a schematic representation, the density profile presented is in very good agreement with detailed models of stellar evolution (Chevalier et al. 2004; Ramirez-Ruiz et al. 2005; Eldridge et al. 2006).

3. BLAST WAVE INTERACTION WITH THE DENSITY DISCONTINUITY AT R_0

We now consider the relativistic blast wave created by the explosion producing the GRB. Since the rest-mass energy of the material in region (b), $E_{\text{RM}} = \dot{M} t_* c^2 \approx 2 \times 10^{54} \dot{M}_{-6} t_{*,6} \text{ ergs}$, is larger than the isotropically equivalent energy released in the explosion producing the GRB, $\sim 10^{53} \text{ ergs}$, the blast wave cannot

² Detailed models of shock propagation into an ambient medium (e.g., Chevalier et al. 2004; Eldridge et al. 2006) suggest that the numerical prefactor depends on early stages of the stellar evolution and may be different than 4. Nonetheless, we show in § 3 that the explosion blast wave is not expected to reach this region while relativistic, and therefore, the exact value of the density in this region has no observational consequences.

³ Note that this equation differs from Wijers (2001) due to an error in the latter.

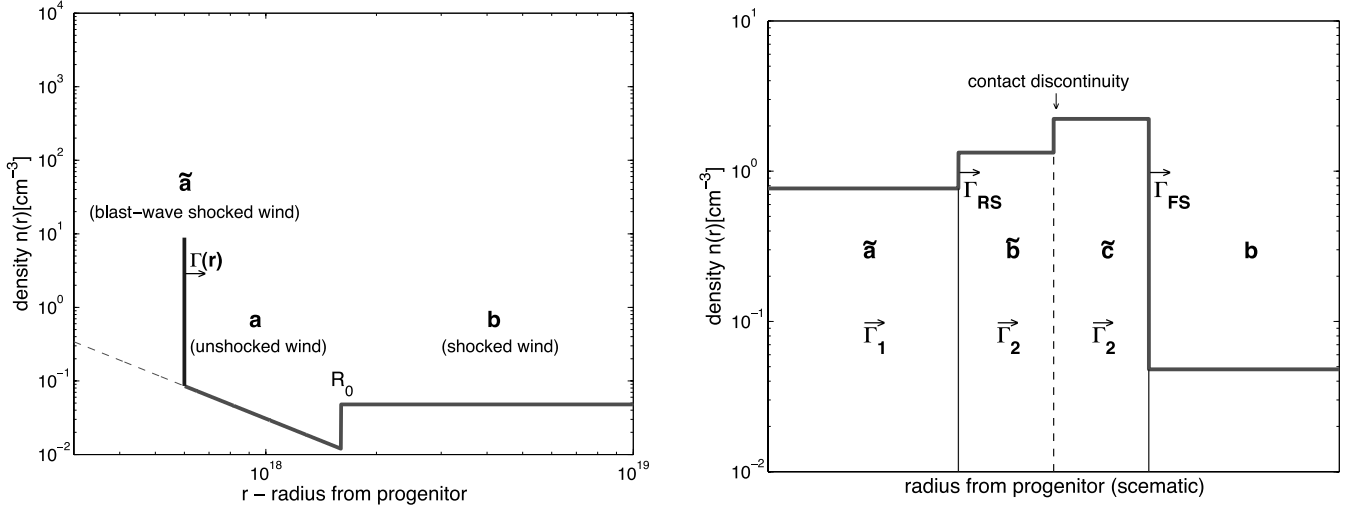


FIG. 2.—Schematic description of the different regimes during the blast wave evolution. *Left*: Blast wave evolution in region (a) results in the creation of region (\tilde{a}), whose observed width $\Delta R \approx r/(4\Gamma^2) \sim 10^{15}$ cm is too narrow to be observed on the scale of the plot. *Right*: Schematic description of the different plasma regimes as the blast wave propagates through $R_0 < r < R_1$, and the reverse shock exists. Region (\tilde{b}) contains plasma from region (\tilde{a}) shocked by the reverse shock, and region (\tilde{c}) contains plasma from region (b) shocked by the forward shock. Here, $\Gamma_1 > \Gamma_2 > \Gamma_{RS}$. [See the electronic edition of the Journal for a color version of this figure.]

cross region (b) while relativistic. Therefore, all the observable effects are expected to occur as the blast wave propagates in regions (a) and (b). In region (a), at radius $r < R_0$, the blast wave evolution is well approximated by the Blandford & McKee (1976) self-similar evolution for an explosion into a density gradient. A similar description holds in region (b) for $r \gg R_0$ (as long as the blast wave remains relativistic). We thus concentrate on the interaction of the blast wave with the density discontinuity at R_0 .

Consider a relativistic blast wave that propagates in region (a). The matter in the downstream region of the shock, which we denote as region (\tilde{a}), is composed of the shocked material of region (a). Being shocked by a relativistic shock wave, its temperature is much higher than $m_e c^2$; thus, the pressure in this region is related to the energy density in the region by the relation $P_{\tilde{a}} = \frac{1}{3}u_{\tilde{a}}$ [as opposed to the relation used in § 2 describing the flow in region (b), $P_b = (2/3)u_b$, which is valid for flow with temperature much smaller than $m_e c^2$, as is the case in region (b) prior to the blast wave propagation]. Since, for $r < R_0$, the fluid in region (\tilde{a}) is downstream from the flow past the shock wave, it thermalizes and hence isotropizes immediately after passing the shock. We therefore adopt the commonly used approximation that the fluid in region (\tilde{a}) is uniform and isotropic. Under this assumption, its number and energy densities are $n_{\tilde{a}}(r) \simeq 4\Gamma(r)n_a(r)$ and $u_{\tilde{a}}(r) \simeq 4\Gamma^2(r)n_a(r)m_p c^2$, respectively, where $\Gamma(r)$ is the Lorentz factor of the flow downstream (see Fig. 2, *left*) and $\Gamma(r) \gg 1$ is assumed (Blandford & McKee 1976).

As the relativistic blast wave reaches R_0 , region (a) no longer exists, and all of its matter is swept up by the shock and is in region (\tilde{a}). At R_0 the blast wave splits into two: a relativistic forward shock that continues to propagate forward into the matter in region (b) and a reverse shock that propagates forward into the matter in region (\tilde{a}). Thus, two new regions are formed: region (\tilde{b}), which contains matter from region (\tilde{a}) shocked by the reverse shock, and region (\tilde{c}), which contains matter from region (b) shocked by the forward shock. Regions (\tilde{b}) and (\tilde{c}) are separated by a contact discontinuity. The fluids in regions (\tilde{b}) and (\tilde{c}) are both at rest relative to the contact discontinuity. Therefore, the fluids in these two regions propagate at the same Lorentz factor Γ_2 (in the observer frame), which is smaller than Γ_1 , the Lorentz factor of the fluid in region (\tilde{a}) at $r = R_0$ (Fig. 2, *right*).

While the relativistic forward shock is strong, the reverse shock thus produced cannot be strong: for a relativistic forward shock, the energy density in region (\tilde{c}) is $u_{\tilde{c}} \simeq 4\Gamma_2^2 \omega_b$, where $\omega_b \simeq n_b m_p c^2$ is the enthalpy in region (b).⁴ For a strong reverse shock, the energy density in region (\tilde{b}) is given by $u_{\tilde{b}} \simeq (4\Gamma_2 + 3)\Gamma_2 \omega_{\tilde{a}}$. Here, $\omega_{\tilde{a}} = (4/3)4\Gamma_1^2 n_a(R_0)m_p c^2$ is the enthalpy in region (\tilde{a}), and Γ_2 is the Lorentz factor of the fluid in region (\tilde{b}) as viewed in the rest frame of region (\tilde{a}), $\Gamma_2 \simeq \frac{1}{2}(\Gamma_1/\Gamma_2 + \Gamma_2/\Gamma_1)$. The term +3 in the expression for $u_{\tilde{b}}$ is added because the Lorentz factor of the fluid in region (\tilde{b}) as viewed in the rest frame of region (\tilde{a}), $\tilde{\Gamma}_2$, is only mildly relativistic. Equating the energy densities at both sides of the contact discontinuity separating regions (\tilde{b}) and (\tilde{c}), using $n_b = 4n_a(R_0)$, leads to $\Gamma_2^2 = \Gamma_2[(4/3)\tilde{\Gamma}_2 + 1]\Gamma_1^2$. Since $\tilde{\Gamma}_2 > 1$, the requirement $\Gamma_2 < \Gamma_1$ cannot be fulfilled. We therefore conclude that the reverse shock formed as the blast wave reaches R_0 is not strong.

The Lorentz factor Γ_2 of the fluid in regions (\tilde{b}) and (\tilde{c}), the number density in region (\tilde{b}), $n_{\tilde{b}}$, and the Lorentz factor of the blast-wave reverse shock, Γ_{RS} , are found using the reverse shock jump conditions and the requirement of pressure balance across the contact discontinuity, which leads to $u_{\tilde{b}} = u_{\tilde{c}}$. We write the Taub adiabatic (e.g., Landau & Lifschitz 1959) at the reverse shock in the form

$$\frac{n_{\tilde{b}}^2}{n_{\tilde{a}}^2} = \frac{\omega_{\tilde{b}}}{\omega_{\tilde{a}}} \left(\frac{\omega_{\tilde{b}} - P_{\tilde{b}} + P_{\tilde{a}}}{\omega_{\tilde{a}} + P_{\tilde{b}} - P_{\tilde{a}}} \right) = \frac{4\Gamma_2^2}{\Gamma_1^2} \left(\frac{\Gamma_1^2 + 12\Gamma_2^2}{3\Gamma_1^2 + 4\Gamma_2^2} \right). \quad (5)$$

Here, $P_{\tilde{a}} = u_{\tilde{a}}/3$ and $P_{\tilde{b}} = u_{\tilde{b}}/3$ are the pressures in regions (\tilde{a}) and (\tilde{b}) [the temperature in region (\tilde{b}) is higher than the temperature in region (\tilde{a}), which is much higher than $m_e c^2$; thus, relativistic formulae are used] respectively; $u_{\tilde{b}} = u_{\tilde{c}} = 4\Gamma_2^2 n_b m_p c^2$ is the energy density in region (\tilde{b}); and $u_{\tilde{a}} = 4\Gamma_1^2 n_a(R_0)m_p c^2$ is the energy density in region (\tilde{a}). The enthalpies in regions (\tilde{a}) and (\tilde{b}) are $\omega_{\tilde{a}} = u_{\tilde{a}} + P_{\tilde{a}}$ and $\omega_{\tilde{b}} = u_{\tilde{b}} + P_{\tilde{b}}$, respectively, and we have used $n_b = 4n_a(R_0)$ in the derivation of the second equality.

⁴ The temperature in region (b) is $T_b \simeq 10^7 v_{w,8}^2$ K (neglecting radiative cooling) and may be lower if radiative cooling is considered (Castor et al. 1975; Ramirez-Ruiz et al. 2005). Therefore, the thermal energy in this region is much smaller than the rest-mass energy, and the pressure is much smaller than the relativistic energy density.

By making a Lorentz transformation from the reverse shock rest frame to the observer frame, conservation of particle number flux at the reverse shock is written in the form

$$\beta_{\text{RS}} = \frac{n_{\tilde{a}}\Gamma_1\beta_1 - n_{\tilde{b}}\Gamma_2\beta_2}{n_{\tilde{a}}\Gamma_1 - n_{\tilde{b}}\Gamma_2} = \frac{(n_{\tilde{a}}/n_{\tilde{b}})\Gamma_1\beta_1 - \Gamma_2\beta_2}{(n_{\tilde{a}}/n_{\tilde{b}})\Gamma_1 - \Gamma_2}, \quad (6)$$

where $\beta_{1,2} \equiv (1 - 1/\Gamma_{1,2}^2)^{1/2}$ is the normalized velocity of the fluid in regions (\tilde{a}) and (\tilde{b}), respectively, and $\beta_{\text{RS}} \equiv (1 - 1/\Gamma_{\text{RS}}^2)^{1/2}$ is the normalized velocity of the reverse shock in the observer frame. As the third equation we use the continuity of the energy flux at the reverse shock, which after Lorentz transformation to the observer frame, takes the form

$$\omega_{\tilde{a}}\Gamma_1^2(1 - \beta_1\beta_{\text{RS}})(\beta_1 - \beta_{\text{RS}}) = \omega_{\tilde{b}}\Gamma_2^2(1 - \beta_2\beta_{\text{RS}})(\beta_2 - \beta_{\text{RS}}). \quad (7)$$

Equations (5), (6), and (7), which connect the thermodynamic properties upstream and downstream of the flow past the reverse shock, are sufficient to calculate the unknown values of the thermodynamic variables Γ_2 , Γ_{RS} , and $n_{\tilde{b}}$. The calculation is done as follows: inserting β_{RS} from equation (6) and using $\omega_{\tilde{b}}/\omega_{\tilde{a}} = 4\Gamma_2^2/\Gamma_1^2$, equation (7) takes the form

$$\begin{aligned} & \Gamma_1^2 \left[\left(\frac{n_{\tilde{a}}}{n_{\tilde{b}}} \right) + \Gamma_1\Gamma_2(\beta_1\beta_2 - 1) \right] \\ &= 4\Gamma_2^2 \left[\left(\frac{n_{\tilde{a}}}{n_{\tilde{b}}} \right) \Gamma_1\Gamma_2(1 - \beta_1\beta_2) - 1 \right] \left(\frac{n_{\tilde{a}}}{n_{\tilde{b}}} \right). \end{aligned} \quad (8)$$

Equation (8) is simplified by approximating $\beta_{1,2} \approx 1 - 1/(2\Gamma_{1,2}^2)$, which leads to

$$2\Gamma_1\Gamma_2 \left(\frac{n_{\tilde{a}}}{n_{\tilde{b}}} \right) (\Gamma_1^2 + 4\Gamma_2^2) = (\Gamma_1^2 + \Gamma_2^2) \left[\Gamma_1^2 + 4\Gamma_2^2 \left(\frac{n_{\tilde{a}}}{n_{\tilde{b}}} \right)^2 \right]. \quad (9)$$

Inserting the ratio $n_{\tilde{a}}/n_{\tilde{b}}$ from equation (5) into equation (9), after some algebra we are left with a quadratic equation for Γ_2^2 ,

$$32\Gamma_2^4 + 8\Gamma_1^2\Gamma_2^2 - 13\Gamma_1^4 = 0, \quad (10)$$

with a solution

$$\begin{aligned} \Gamma_2^2 &= \frac{\sqrt{27} - 1}{8} \Gamma_1^2, \\ \Gamma_2 &\simeq 0.725\Gamma_1. \end{aligned} \quad (11)$$

Inserting this result in equation (5), the number density in region (\tilde{b}) is given by

$$\frac{n_{\tilde{b}}^2}{n_{\tilde{a}}^2} = \frac{153\sqrt{3} - 259}{2} \approx 3, \quad (12)$$

or $n_{\tilde{b}} \simeq 1.73n_{\tilde{a}}$. The energy density in region (\tilde{b}) is

$$\frac{\omega_{\tilde{b}}}{\omega_{\tilde{a}}} = \frac{u_{\tilde{b}}}{u_{\tilde{a}}} = \frac{4\Gamma_2^2}{\Gamma_1^2} = \frac{3\sqrt{3} - 1}{2} \approx 2.1, \quad (13)$$

which means that the energy per particle in region (\tilde{b}) is $u_{\tilde{b}}/n_{\tilde{b}} \simeq (2.1/1.73)u_{\tilde{a}}/n_{\tilde{a}} \approx 1.21u_{\tilde{a}}/n_{\tilde{a}}$. We therefore conclude that the energy per particle is increased by $\sim 20\%$ as the particle passes

through the reverse shock from region (\tilde{a}) to (\tilde{b}). The Lorentz factor of the reverse shock is calculated using equation (6),

$$\Gamma_{\text{RS}} \simeq 0.43\Gamma_1. \quad (14)$$

4. BLAST WAVE EVOLUTION

As long as the explosion blast wave propagates in region (a) at $r < R_0$, its evolution is well described by the Blandford & McKee (1976) self-similar solution for an explosion into a density gradient $n(r) \propto r^{-2}$,

$$\Gamma(r; r < R_0) = \left(\frac{9E}{16\pi A c^2} \right)^{1/2} \frac{1}{r^{1/2}}, \quad (15)$$

where E is the (isotropically equivalent) explosion energy and $A \equiv \dot{M}/(4\pi v_w)$. At $r = R_0$,

$$\Gamma_1 \equiv \Gamma(r = R_0) = 20.5E_{53}^{1/2} n_{R_0, -1.5}^{-1/2} R_{0,18}^{-3/2}, \quad (16)$$

where $n_a(R_0) = 10^{-1.5} n_{R_0, -1.5} \text{ cm}^{-3}$.

The spatial dependence of the hydrodynamic variables of a shocked fluid element [in region (\tilde{a})] is given by the Blandford & McKee (1976) self-similar solution. In this solution, as the blast wave expands to radius r , more than 90% of the energy and the particles are concentrated in a shell of comoving thickness $\Delta r_a^{\text{co}} = \xi r/\Gamma(r)$, where ξ is a numerical factor in the approximate range 0.1–0.5 for the hydrodynamic quantity in question (number density, energy, Lorentz factor, etc.). Adopting the approximation that the fluid in region (\tilde{a}) is homogeneously distributed, we write the comoving width of this region at $r = R_0$ as $\Delta R_a^{\text{co}}(r = R_0) = R_0/8\zeta\Gamma_1$, where ζ is a numerical factor of order unity, which is inserted in order to parameterize the discrepancy between the actual density and energy profiles and the homogeneity approximation used. The Lorentz factor of each fluid element in region (\tilde{a}) at $r = R_0$ is therefore approximated to be $\Gamma(r = R_0) = \Gamma_1$.

At $r > R_0$, the flow in region (\tilde{a}), which was downstream the flow past the blast wave at $r < R_0$, becomes upstream the flow past the reverse shock. A fluid element in region (\tilde{a}) therefore continues to move at an approximately constant (r -independent) Lorentz factor $\Gamma = \Gamma_1$, as long as the reverse shock exists.⁵ The shock jump conditions analyzed in § 3 then imply that the Lorentz factor of a fluid element in regions (\tilde{b}) and (\tilde{c}) is also r -independent, given by equation (11), $\Gamma_2 = 0.725\Gamma_1 = 14.8E_{53}^{1/2} n_{R_0, -1.5}^{-1/2} R_{0,18}^{-3/2}$.

The Lorentz factor of the reverse shock during its lifetime is determined by the reverse shock jump conditions as well, hence is r -independent, and is given by equation (14), $\Gamma_{\text{RS}} = 0.43\Gamma_1 = 8.8E_{53}^{1/2} n_{R_0, -1.5}^{-1/2} R_{0,18}^{-3/2}$. The reverse shock therefore completes its crossing through region (\tilde{a}) at a distance

$$R_1 = R_0 + \frac{\Delta R_a^{\text{ob}}(r = R_0)}{\beta_1 - \beta_{\text{RS}}} \simeq R_0 \left(1 + \frac{1}{17.6\zeta} \right) = 1.06R_0 \quad (17)$$

from the explosion. Here, $\Delta R_a^{\text{ob}}(r = R_0) = \Delta R_a^{\text{co}}(r = R_0)/\Gamma_1$ is the observer-frame width of region (\tilde{a}) at $r = R_0$, and $\zeta = 1$ is assumed in the last equality. At $r > R_1$ region (\tilde{a}) no longer exists, as all of its content is in region (\tilde{b}), and the reverse shock disappears.

⁵ The velocity of the reverse shock in the rest frame of region (\tilde{a}), $\tilde{\beta}_{\text{RS}} = 0.69$, is of course larger than the speed of sound, $\beta_{\text{sound}} = 0.57$. We therefore do not expect a significant change in the thermodynamic properties of region (\tilde{a}) due to adiabatic expansion during the reverse shock crossing time.

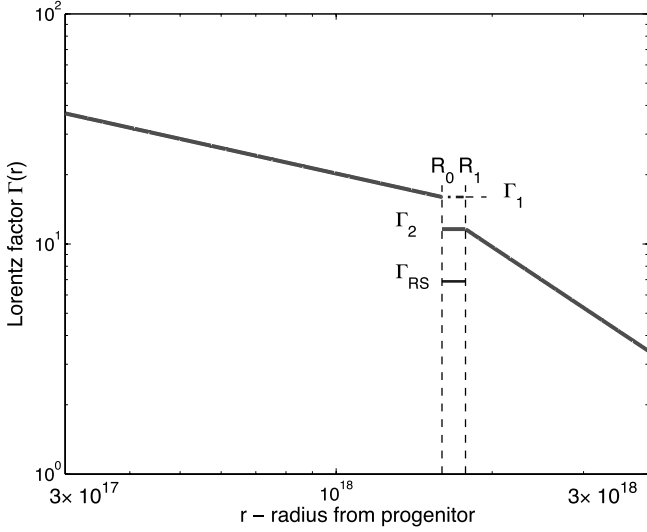


FIG. 3.—Schematic description of the plasma Lorentz factor as a function of r . For $r < R_0$, $\Gamma(r) \propto r^{-1/2}$, at $R_0 < r < R_1$, plasma in region (*a*) continues to move at $\Gamma_1 \equiv \Gamma(r = R_0)$, while plasma in regions (*b*) and (*c*) moves at Lorentz factor $\Gamma_2 = 0.725\Gamma_1$. The reverse shock moves at Lorentz factor $\Gamma_{RS} = 0.43\Gamma_1$. At $r > R_1$, plasma in regions (*b*) and (*c*) moves in a self-similar motion with Lorentz factor $\Gamma \propto r^{-3/2}$. [See the electronic edition of the *Journal* for a color version of this figure.]

The total mass of the matter swept up by the blast wave as it propagates from R_0 to R_1 is

$$m_b(r = R_1) = \frac{4\pi}{3} m_p n_b (R_1^3 - R_0^3) = \frac{4}{3} \left[\left(\frac{R_1}{R_0} \right)^3 - 1 \right] m_a \simeq 0.24 m_a, \quad (18)$$

where $m_a = 4\pi m_p \int_{r=0}^{R_0} n_a(r) r^2 dr$ is the total swept-up mass of region (*a*). The thermal energy of the particles swept up as the blast wave propagates from R_0 to R_1 , $E_{th} \simeq \Gamma_2^2 m_b c^2$ (assuming no radiative losses), is much larger than the fluids' kinetic energy at R_1 , $E_k \simeq \Gamma_2 (m_a + m_b) c^2$. As long as the reverse shock exists, the energy excess is compensated by kinetic energy loss of particles moving through the reverse shock from region (*a*) to region (*b*). At $r > R_1$ the reverse shock no longer exists, and therefore the plasma decelerates. Since at this stage the thermal energy is already much larger than the kinetic energy, a self-similar expansion follows soon after the reverse shock ceases to exist, at $r \simeq R_1$. This self-similar expansion is well described by the Blandford & McKee (1976) solution for an expansion into a uniform density medium. We thus conclude that at $r > R_1$, the fluid Lorentz factor is given by $\Gamma(r > R_1) = \Gamma_2 (r/R_1)^{-3/2}$.

The evolutionary stages of the fluid's Lorentz factor in the different regimes are summarized in Figure 3. The initial blast wave exists at $r < R_0$. At $R_0 < r < R_1$, fluid in region (*a*) moves at a constant Lorentz factor Γ_1 , while fluid in regions (*b*) and (*c*) moves at a constant Lorentz factor Γ_2 . At $r > R_1$, the fluid occupies regions (*b*) and (*c*) only and moves in a self-similar motion. The blast wave becomes nonrelativistic ($\Gamma_2 - 1 \simeq 1$) at radius $R_{NR} \simeq 3.3R_1 \simeq 3.5 \times 10^{18} R_{0,18}$ cm.

5. AFTERGLOW REBRIGHTENING

The complex dynamic of the blast wave evolution has observational consequences. In this section, we calculate the expected light curve in this scenario. In our calculations, we use the standard synchrotron emission model, which is in very good agreement with afterglow observations (e.g., Wijers et al. 1997;

van Paradijs et al. 2000). We divide the calculation of the emitted radiation into the three different phases, corresponding to the three phases of the blast wave evolution: (1) the earliest phase, which corresponds to blast wave evolution in the innermost regime, $r < R_0$; (2) the intermediate phase, corresponding to the forward and reverse shock wave evolution at $R_0 < r < R_1$; and (3) the latest phase, corresponding to blast wave propagation at $r > R_1$.

5.1. Emission during the Early Phase, $r < R_0$

The Lorentz factor of the shocked plasma [in region (*a*)] at $r < R_0$ is given by equation (15). The characteristic time at which radiation emitted by shocked plasma at radius r is observed by a distant observer was calculated by Waxman (1997) for the case of an explosion into a uniform medium, $t^{ob} \approx r/4\Gamma^2 c$. Repeating the Waxman (1997) calculation for the case of an explosion into a density gradient $n(r) \propto r^{-2}$, we show in the Appendix that in this case this relation is slightly modified, $t^{ob} \approx r/2\Gamma^2 c$. Radiation observed at time t^{ob} is therefore emitted as the blast wave approaches radius $r = (9Et^{ob}/8\pi Ac)^{1/2}$. Radiation emitted at $r = R_0$ is observed at time

$$t_0^{ob} = \frac{8\pi Ac}{9E} R_0^2 \simeq 4.08 \times 10^4 E_{53}^{-1} n_{R_0,-1.5} R_{0,18}^4 \text{ s}, \quad (19)$$

or about 0.47 days after the explosion.

Denoting by ϵ_e and ϵ_B the fractions of postshock thermal energy density, $u_{int} = 4\Gamma^2(r) n_a(r) m_p c^2$, that are carried by the electrons and the magnetic field, respectively, the magnetic field (in the fluid frame) is given by

$$B(t^{ob} < t_0^{ob}) = \left[8\pi\epsilon_B \left(\frac{9E}{4\pi} \right) \left(\frac{8\pi Ac}{9Et^{ob}} \right)^{3/2} \right]^{1/2} \\ = 7.7 \times 10^{-2} E_{53}^{-1/4} \epsilon_{B,-2}^{1/2} t_{\text{day}}^{ob,-3/4} n_{R_0,-1.5}^{3/4} R_{0,18}^{3/2} \text{ G}, \quad (20)$$

where $t^{ob} = 1 t_{\text{day}}^{ob}$. The characteristic Lorentz factor of the shock wave accelerated electrons is $\gamma_{\text{char}} \simeq \epsilon_e (m_p/m_e) \Gamma(r) [(p-2)/(p-1)]$, where p is the power-law index of the accelerated electron energy distribution, $n_e(\gamma) \propto \gamma^{-p}$ for $\gamma > \gamma_{\text{char}}$. The resulting synchrotron emission peaks at

$$\nu_m^{ob}(t^{ob} < t_0^{ob}) = 5.6 \times 10^{12} (1+z)^{-1} E_{53}^{1/2} \epsilon_{e,-1}^{1/2} \epsilon_{B,-2}^{1/2} t_{\text{day}}^{ob,-3/2} \text{ Hz}, \quad (21)$$

where z is the redshift, characteristic values $\epsilon_e = 10^{-1} \epsilon_{e,-1}$ and $\epsilon_B = 10^{-2} \epsilon_{B,-2}$ are taken (e.g., Wijers & Galama 1999), and a power-law index $p = 2.5$ is assumed. This frequency is below the break frequency of the spectrum, corresponding to emission from electrons for which the synchrotron cooling time is equal to the dynamical time, $t_{\text{dyn}} \sim r/8\zeta c \Gamma(r)$,

$$\nu_c^{ob}(t^{ob} < t_0^{ob}) = 7.2 \times 10^{17} (1+z)^{-1} \\ \times E_{53}^{1/2} \epsilon_{B,-2}^{-3/2} \zeta_0^{1/2} t_{\text{day}}^{ob,1/2} n_{R_0,-1.5}^{-2} R_{0,18}^{-4} \text{ Hz}. \quad (22)$$

The synchrotron self-absorption frequency is

$$\nu_{\text{ssa}}^{ob}(t^{ob} < t_0^{ob}) = 7.8 \times 10^8 (1+z)^{-1} \\ \times E_{53}^{-2/5} \epsilon_{e,-1}^{-1} \epsilon_{B,-2}^{1/5} \zeta_0^{-3/5} t_{\text{day}}^{ob,-3/5} n_{R_0,-1.5}^{6/5} R_{0,18}^{12/5} \text{ Hz}. \quad (23)$$

The maximum Lorentz factor of the accelerated electrons is given by equating the synchrotron loss time to the acceleration time, $t_{\text{acc}} \simeq E/(cqB)$. Synchrotron emission from these electrons peaks at

$$\nu_{\text{max}}^{\text{ob.}}(t^{\text{ob.}} < t_0^{\text{ob.}}) = 9.6 \times 10^{23} (1+z)^{-1} E_{53}^{1/4} t_{\text{day}}^{-1/4} n_{R_{0,-1.5}}^{-1/4} R_{0,18}^{-1/2} \text{ Hz.} \quad (24)$$

Finally, the observed specific flux at $\nu_m^{\text{ob.}}$ is given by the number of radiating electrons $N_{\text{TOT}}(r) = 4\pi Ar/m_p$ times the observed power (per unit frequency, at $\nu_m^{\text{ob.}}$) of a single electron $\Gamma(r)\sqrt{3}q^3 B/m_e c^2$ divided by $4\pi d_L^2$,

$$F_{\text{max}}(t^{\text{ob.}} < t_0^{\text{ob.}}) = 12.7 E_{53}^{1/2} \epsilon_{B,-2}^{1/2} t_{\text{day}}^{\text{ob.}-1/2} d_{L,28}^{-2} n_{R_{0,-1.5}} R_{0,18}^2 \text{ mJy,} \quad (25)$$

where $d_L = 10^{28} d_{L,28}$ cm is the luminosity distance to the GRB.

5.2. Emission in the Intermediate Phase, $R_0 < r < R_1$

At $t_0^{\text{ob.}}$ the blast wave reaches R_0 and splits into the relativistic forward and reverse shock waves. As we showed in § 4, the Lorentz factor of the plasma is r -independent in this regime. We show in the Appendix that in this case the time delay suffered by photons emitted at radius r compared to photons emitted at $r = 0$ is $\Delta t^{\text{ob.}} \approx r/\Gamma^2(r)c$. We thus find that this phase lasts a duration

$$\Delta t^{\text{ob.}} \equiv t_1^{\text{ob.}} - t_0^{\text{ob.}} = \frac{R_1 - R_0}{\Gamma^2 c} = 8.58 \times 10^3 E_{53}^{-1} \zeta_0^{-1} n_{R_{0,-1.5}} R_{0,18}^4 \text{ s,} \quad (26)$$

or about 0.10 days.

For $R_0 < r < R_1$ there are three distinctive emitting regions: particles in region (\tilde{a}) that were the only source of emission at $r < R_0$ continue to emit, particles in region (\tilde{b}) that crossed the reverse shock and were reheated by it, and particles in region (\tilde{c}) that are heated by the forward shock. All these regions are characterized by different thermodynamic quantities, and therefore the emission pattern in each region is unique. We thus calculate separately emission from the different regions.

5.2.1. Emission from Particles in Region (\tilde{a})

Region (\tilde{a}), which was downstream of the flow past the blast wave at $r < R_0$, becomes upstream of the flow past the reverse shock at $r > R_0$. For $r > R_0$, the fluid can therefore only leave this region; high-energy particles are no longer injected into the region, and no information enters it. The thermodynamic properties of the flow (e.g., energy density, magnetic field, etc.) “freeze out” at their values at $r = R_0$. The values of the peak frequency and of the spectral break frequency are therefore equal to their values at $t^{\text{ob.}} = t_0^{\text{ob.}}$,

$$\nu_m^{\text{ob.}}(\tilde{a}; t_0^{\text{ob.}} < t^{\text{ob.}} < t_1^{\text{ob.}}) = 1.8 \times 10^{13} (1+z)^{-1} \times E_{53}^2 \epsilon_{e,-1}^2 \epsilon_{B,-2}^{1/2} n_{R_{0,-1.5}}^{-3/2} R_{0,18}^{-6} \text{ Hz,} \quad (27)$$

$$\nu_c^{\text{ob.}}(\tilde{a}; t_0^{\text{ob.}} < t^{\text{ob.}} < t_1^{\text{ob.}}) = 4.9 \times 10^{17} (1+z)^{-1} \times \epsilon_{B,-2}^{-3/2} \zeta_0^2 n_{R_{0,-1.5}}^{-3/2} R_{0,18}^{-2} \text{ Hz.} \quad (28)$$

The comoving width of region (\tilde{a}) decreases linearly from its width at t_0 , $\Delta R_{\tilde{a}}^{\text{co.}}(t = t_0) = c\Gamma_1 t_0^{\text{ob.}}/4\zeta$, to 0 at $t_1^{\text{ob.}}$. Therefore,

the optical depth decreases linearly with time, and the synchrotron self-absorption frequency is given by⁶

$$\nu_{\text{ssa}}^{\text{ob.}}(\tilde{a}; t_0^{\text{ob.}} < t^{\text{ob.}} < t_1^{\text{ob.}}) = 1.2 \times 10^9 \left(\frac{t_1^{\text{ob.}} - t^{\text{ob.}}}{t_1^{\text{ob.}} - t_0^{\text{ob.}}} \right)^{3/5} (1+z)^{-1} \times E_{53}^{1/5} \epsilon_{e,-1}^{-1/5} \epsilon_{B,-2}^{1/5} \zeta_0^{-3/5} n_{R_{0,-1.5}}^{3/5} \text{ Hz.} \quad (29)$$

Since energetic electrons are not injected into this region at $t^{\text{ob.}} > t_0^{\text{ob.}}$, the highest energy electrons, having Lorentz factor $\gamma_{\text{max}}(t^{\text{ob.}} = t_0^{\text{ob.}}) = 3.2 \times 10^8 E_{53}^{-1/4} \epsilon_{B,-2}^{1/4} R_{0,18}^{3/4}$ at $t^{\text{ob.}} = t_0^{\text{ob.}}$, cool by synchrotron radiation. Synchrotron emission from these electrons peaks at

$$\nu_{\text{max}}^{\text{ob.}}(\tilde{a}; t_0^{\text{ob.}} < t^{\text{ob.}} < t_1^{\text{ob.}}) = \min \left[\nu_{\text{max}}^{\text{ob.}}(t^{\text{ob.}} = t_0^{\text{ob.}}), \frac{4.4 \times 10^{27}}{(t^{\text{ob.}} - t_0^{\text{ob.}})^2} (1+z)^{-1} E_{53}^{-2} \epsilon_{B,-2}^{-3/2} \zeta_0^2 n_{R_{0,1.5}}^{1/2} R_{0,18}^6 \text{ Hz} \right], \quad (30)$$

where $\nu_{\text{max}}^{\text{ob.}}(t^{\text{ob.}} = t_0^{\text{ob.}}) = 1.1 \times 10^{24} (1+z)^{-1} E_{53}^{1/2} n_{R_{0,-1.5}}^{-1/2} R_{0,18}^{-3/2}$ Hz is the frequency of the synchrotron emitted photons from the most energetic electrons at $t^{\text{ob.}} = t_0^{\text{ob.}}$. At $t^{\text{ob.}} = t_1^{\text{ob.}}$,

$$\nu_{\text{max}}^{\text{ob.}}(\tilde{a}; t^{\text{ob.}} = t_1^{\text{ob.}}) = 6.0 \times 10^{19} (1+z)^{-1} \epsilon_{B,-2}^{-3/2} \zeta_0^4 n_{R_{0,-1.5}}^{-3/2} R_{0,18}^{-2} \text{ Hz.} \quad (31)$$

The reverse shock crosses this region at constant velocity; therefore, the number of radiating electrons in this region decreases linearly with time. As a result, the total flux at $\nu_m^{\text{ob.}}$ decreases linearly from its value at $t^{\text{ob.}} = t_0^{\text{ob.}}$, $F_{\text{max}}(\tilde{a}; t^{\text{ob.}} = t_0^{\text{ob.}}) = 18.5 E_{53} \epsilon_{B,-2}^{1/2} d_{L,28}^{-2} n_{R_{0,-1.5}}^{1/2}$ mJy, to 0 at $t^{\text{ob.}} = t_1^{\text{ob.}}$.

5.2.2. Emission from Particles in Region (\tilde{b})

Assuming that similar fractions $\epsilon_B = 10^{-2}$ of the postshock thermal energy are converted to magnetic field at both the reverse and the forward shock waves, the magnetic field produced by the reverse shock wave,

$$B_{\tilde{b}}(\text{prod.}) = [8\pi \epsilon_B u_{\tilde{b}}(t^{\text{ob.}} > t_0^{\text{ob.}})]^{1/2} = \{8\pi \epsilon_B [2.1 u_{\tilde{a}}(t^{\text{ob.}} > t_0^{\text{ob.}})]\}^{1/2}, \quad (32)$$

(see eq. [13]) is smaller than the magnetic field advected with the flow from region (\tilde{a}),

$$B_{\tilde{b}}(\text{adv.}) = \frac{n_{\tilde{b}}}{n_{\tilde{a}}} B_{\tilde{a}}(t^{\text{ob.}} > t_0^{\text{ob.}}) = \sqrt{3} B_{\tilde{a}}(t^{\text{ob.}} > t_0^{\text{ob.}}) = 0.23 E_{53}^{1/2} \epsilon_{B,-2}^{1/2} R_{0,18}^{-3/2} \text{ G,} \quad (33)$$

by a factor $(3/2.1)^{1/2} \approx 1.2$. Here, the energy density and the magnetic field in region (\tilde{a}) assume their value at $t_0^{\text{ob.}}$ for $t^{\text{ob.}} > t_0^{\text{ob.}}$. We therefore assume that the magnetic field in this region is equal to the advected magnetic field, given by equation (33).

The reheating of the plasma by the reverse shock implies that the characteristic Lorentz factor of the electrons in this region is larger by a factor $(u_{\tilde{b}}/n_{\tilde{b}})/(u_{\tilde{a}}/n_{\tilde{a}}) = 2.1/1.73 = 1.21$ than the

⁶ The photons have to cross several layers of plasma [regions (\tilde{b}) and (\tilde{c})] before reaching the observer. The observed self-absorption frequency therefore depends on the plasma parameters in the different regions.

characteristic Lorentz factor of electrons in region (\tilde{a}). The characteristic synchrotron emission thus peaks at

$$\nu_m^{\text{ob}}(\tilde{b}; t_0^{\text{ob}} < t^{\text{ob}} < t_1^{\text{ob}}) = 3.2 \times 10^{13} (1+z)^{-1} \times E_{53}^2 \epsilon_{e,-1}^2 \epsilon_{B,-2}^{1/2} n_{R_0,-1.5}^{-3/2} R_{0,18}^{-6} \text{ Hz.} \quad (34)$$

The reverse shock rerandomizes the energy; thus, the spectral break frequency is independent of the break frequency in region (\tilde{a}) and is given by

$$\nu_c^{\text{ob}}(\tilde{b}; t_0^{\text{ob}} < t^{\text{ob}} < t_1^{\text{ob}}) = \frac{8.6 \times 10^{26}}{(t^{\text{ob}} - t_0^{\text{ob}})^2} (1+z)^{-1} \times E_{53}^{-2} \epsilon_{B,-2}^{-3/2} \zeta_0^2 n_{R_0,-1.5}^{1/2} R_{0,18}^6 \text{ Hz.} \quad (35)$$

At $t^{\text{ob}} = t_0^{\text{ob}}$, the comoving width of this region is 0; hence the break frequency $\nu_c^{\text{ob}}(\tilde{b}; t_0^{\text{ob}} \rightarrow t^{\text{ob}}) \rightarrow \infty$. At $t^{\text{ob}} = t_1^{\text{ob}}$, this frequency is equal to

$$\nu_c^{\text{ob}}(\tilde{b}; t^{\text{ob}} = t_1^{\text{ob}}) = 1.2 \times 10^{19} (1+z)^{-1} \epsilon_{B,-2}^{-3/2} \zeta_0^4 n_{R_0,-1.5}^{-3/2} R_{0,18}^{-2} \text{ Hz.} \quad (36)$$

The self-absorption frequency is

$$\nu_{\text{ssa}}^{\text{ob}}(\tilde{b}; t_0^{\text{ob}} < t^{\text{ob}} < t_1^{\text{ob}}) = 1.1 \times 10^6 (t^{\text{ob}} - t_0^{\text{ob}})^{3/5} (1+z)^{-1} E_{53}^{4/5} \epsilon_{e,-1}^{-1} \epsilon_{B,-2}^{1/5} \zeta_0^{-3/5} R_{0,18}^{-12/5} \text{ Hz,} \quad (37)$$

while the highest frequency of the synchrotron emitted photons is expected at

$$\nu_{\text{max}}^{\text{ob}}(\tilde{b}; t_0^{\text{ob}} < t^{\text{ob}} < t_1^{\text{ob}}) = 8.5 \times 10^{23} (1+z)^{-1} \times E_{53}^{1/2} n_{R_0,-1.5}^{-1/2} R_{0,18}^{-3/2} \text{ Hz.} \quad (38)$$

The observed flux at ν_m^{ob} emitted from this region is expected to grow linearly from 0 at t_0^{ob} to

$$\begin{aligned} F_{\text{max}}(\tilde{b}; t^{\text{ob}} = t_1^{\text{ob}}) &= \frac{B_{\tilde{b}} \Gamma_2}{B_{\tilde{a}} \Gamma_1} F_{\text{max}}(\tilde{a}; t^{\text{ob}} = t_0^{\text{ob}}) \\ &= \sqrt{3} [0.725 F_{\text{max}}(\tilde{a}; t^{\text{ob}} = t_0^{\text{ob}})] \\ &= 23.2 E_{53} \epsilon_{B,-2}^{1/2} d_{L,28}^{-2} n_{R_0,-1.5}^{1/2} \text{ mJy} \end{aligned} \quad (39)$$

at $t^{\text{ob}} = t_1^{\text{ob}}$.

5.2.3. Emission from Particles in Region (\tilde{c})

While the energy density in region (\tilde{c}) is equal to the energy density in region (\tilde{b}), there is no advected magnetic field term. Hence, the magnetic field in this region is assumed to be produced by the forward shock and is equal to $B_{\tilde{c}} = B_{\tilde{b}}(\text{adv.})/1.2 = 1.9 \times 10^{-1} E_{53}^{1/2} \epsilon_{B,-2}^{1/2} R_{0,18}^{-3/2} \text{ G}$ (see eq. [33]). Electrons are accelerated by the forward shock to a characteristic Lorentz factor $\gamma_{\text{char}}(\tilde{c}) \simeq \epsilon_e (m_p/m_e) \Gamma_2 [(p-2)/(p-1)]$, producing synchrotron radiation at a characteristic frequency,

$$\nu_m^{\text{ob}}(\tilde{c}; t_0^{\text{ob}} < t^{\text{ob}} < t_1^{\text{ob}}) = 1.0 \times 10^{13} (1+z)^{-1} \times E_{53}^2 \epsilon_{e,-1}^2 \epsilon_{B,-2}^{1/2} n_{R_0,-1.5}^{-3/2} R_{0,18}^{-6} \text{ Hz.} \quad (40)$$

The characteristic spectral break frequency is $\nu_c^{\text{ob}}(\tilde{c}) = \nu_c^{\text{ob}}(\tilde{b}) (B_{\tilde{b}}/B_{\tilde{c}})^3$, or

$$\nu_c^{\text{ob}}(\tilde{c}; t_0^{\text{ob}} < t^{\text{ob}} < t_1^{\text{ob}}) = \frac{1.5 \times 10^{27}}{(t^{\text{ob}} - t_0^{\text{ob}})^2} (1+z)^{-1} \times E_{53}^{-2} \epsilon_{B,-2}^{-3/2} \zeta_0^2 n_{R_0,-1.5}^{1/2} R_{0,18}^6 \text{ Hz,} \quad (41)$$

which is equal to

$$\begin{aligned} \nu_c^{\text{ob}}(\tilde{c}; t^{\text{ob}} = t_1^{\text{ob}}) &= 2.0 \times 10^{19} (1+z)^{-1} \epsilon_{B,-2}^{-3/2} \zeta_0^4 n_{R_0,-1.5}^{-3/2} R_{0,18}^{-2} \text{ Hz} \end{aligned} \quad (42)$$

at $t^{\text{ob}} = t_1^{\text{ob}}$. The synchrotron self-absorption frequency is given by

$$\begin{aligned} \nu_{\text{ssa}}^{\text{ob}}(\tilde{c}; t_0^{\text{ob}} < t^{\text{ob}} < t_1^{\text{ob}}) &= 2.5 \times 10^6 (t^{\text{ob}} - t_0^{\text{ob}})^{3/5} (1+z)^{-1} E_{53}^{4/5} \epsilon_{e,-1}^{-1} \epsilon_{B,-2}^{1/5} \zeta_0^{-3/5} R_{0,18}^{-12/5} \text{ Hz,} \end{aligned} \quad (43)$$

and the highest frequency of the synchrotron emitted photons is independent of the magnetic field strength and therefore equals the highest frequency of the synchrotron emitted photons in region (\tilde{b}), $\nu_{\text{max}}^{\text{ob}}(\tilde{c}; t_0^{\text{ob}} < t^{\text{ob}} < t_1^{\text{ob}}) = \nu_{\text{max}}^{\text{ob}}(\tilde{b}; t_0^{\text{ob}} < t^{\text{ob}} < t_1^{\text{ob}})$ (see eq. [38]).

The number of particles swept by the forward shock from region (b) into this region grows linearly with time and is equal to $N_2 = 4\pi \int_{R_0}^{R_1} r^2 n_b dr = (4/3) N_1 [(R_1/R_0)^3 - 1] \approx 0.24 N_1 \zeta_0^{-1}$ at $r = R_1$ (see eq. [18]). Here, $N_1 = 4\pi A R_0 / m_p$ is the total number of particles in region (a) that were swept by the blast wave at $r = R_0$. The observed flux at ν_m^{ob} emitted from this region therefore grows linearly with time from 0 at t_0^{ob} to

$$F_{\text{max}}(\tilde{c}; t^{\text{ob}} = t_1^{\text{ob}}) = 4.8 E_{53} \epsilon_{B,-2}^{1/2} d_{L,28}^{-2} n_{R_0,-1.5}^{1/2} \text{ mJy,} \quad (44)$$

at $t^{\text{ob}} = t_1^{\text{ob}}$.

5.3. Emission in the Latest Phase, $r > R_1$

As explained in § 4, the blast wave evolution at $r > R_1$ is approximated by the self-similar evolution, $\Gamma(r > R_1) = \Gamma_2 (r/R_1)^{-3/2}$. At $r = R_1$, the shocked shell contains matter shocked by the reverse shock in region (\tilde{b}), as well as matter shocked by the forward shock in region (\tilde{c}). While for $r > R_1$ hot matter continues to enter region (\tilde{c}) through the forward shock wave, matter in region (\tilde{b}) cools adiabatically. Therefore, the energy densities of the flow at the two sides of the contact discontinuity that separates regions (\tilde{b}) and (\tilde{c}) are different for $r > R_1$. For an explosion into a constant-density medium, the energy density in region (\tilde{c}) evolves as $u_{\tilde{c}} \propto \Gamma^2(r) n(r) \propto r^{-3}$, while the energy density in region (\tilde{b}) is $u_{\tilde{b}} \propto r^{-4}$. It thus follows that the contact discontinuity cannot separate these regions anymore. Matter in these two regions starts to mix at $r > R_1$, and region (\tilde{b}) eventually disappears.

We thus treat the matter in regions (\tilde{b}) and (\tilde{c}) as having similar thermodynamic properties at $r > R_1$. This matter is concentrated in a shell, whose observed width at $r = R_1$ is $\Delta R(r = R_1) = c \Delta t^{\text{ob}} (\beta_2 - \beta_{\text{RS}}) = 0.20 R_1 / (4\Gamma_2^2)$. During the self-similar motion that follows, the width of the shell is $\Delta R \propto t^{\text{ob}}$. We therefore expect that the shell's width increases to its terminal value $\Delta R(r) = r / [4\Gamma^2(r)]$ by sweeping matter into region (\tilde{c}), shortly

after $t_1^{\text{ob.}}$. We therefore neglect emission from region (\tilde{b}) compared to emission from region (\tilde{c}) at $r > R_1$, as well as the numerical factor 0.20, and calculate the emission in the latest evolutionary phase in accordance to the self-similar solution, which is the asymptotic solution for $r \gg R_1$.

The time delay suffered by photons emitted in this region compared to photons emitted at $r = 0$ is therefore $\Delta t^{\text{ob.}} \approx r/4\Gamma^2(r)c$; hence, the time delay compared to photons emitted at R_1 is $\Delta t^{\text{ob.}} - R_1/(4\Gamma_2^2 c)$. These photons are therefore seen at time

$$t^{\text{ob.}} = t_1^{\text{ob.}} - \frac{R_1}{4\Gamma_2^2 c} + \frac{r}{4\Gamma^2(r)c} \quad (45)$$

from the explosion. This equation is written in the form

$$\tilde{t}^{\text{ob.}} = \frac{r}{4\Gamma^2 c}, \quad (46)$$

where $\tilde{t}^{\text{ob.}} \equiv t^{\text{ob.}} - t_1^{\text{ob.}} + R_1/(4\Gamma_2^2 c)$.

Using this scaling, the magnetic field is given by

$$\begin{aligned} B(t^{\text{ob.}} > t_1^{\text{ob.}}) &= (8\pi\epsilon_B 4\Gamma^2 n_b m_p c^2)^{1/2} \\ &= 0.15 E_{53}^{1/8} \epsilon_{B,-2}^{1/2} (\tilde{t}_{\text{day}}^{\text{ob.}})^{-3/8} n_{R_0,-1.5}^{3/8} \text{ G}, \end{aligned} \quad (47)$$

where $\tilde{t}^{\text{ob.}} = 1\tilde{t}_{\text{day}}^{\text{ob.}}$ day. Synchrotron radiation therefore peaks at

$$\nu_m^{\text{ob.}}(t^{\text{ob.}} > t_1^{\text{ob.}}) = 3.5 \times 10^{12} (1+z)^{-1} E_{53}^{1/2} \epsilon_{e,-1}^2 \epsilon_{B,-2}^{1/2} (\tilde{t}_{\text{day}}^{\text{ob.}})^{-3/2} \text{ Hz}. \quad (48)$$

The break frequency in the spectrum is at

$$\begin{aligned} \nu_c^{\text{ob.}}(t^{\text{ob.}} > t_1^{\text{ob.}}) &= 3.2 \times 10^{16} (1+z)^{-1} \\ &\times E_{53}^{-1/2} \epsilon_{B,-2}^{-3/2} \zeta_0^2 (\tilde{t}_{\text{day}}^{\text{ob.}})^{-1/2} n_{R_0,-1.5}^{-1} \text{ Hz}, \end{aligned} \quad (49)$$

and the self-absorption frequency is

$$\begin{aligned} \nu_{\text{ssa}}^{\text{ob.}}(t^{\text{ob.}} > t_1^{\text{ob.}}) &= 3.5 \times 10^9 (1+z)^{-1} \\ &\times E_{53}^{1/5} \epsilon_{e,-1}^{-1} \epsilon_{B,-2}^{1/5} \zeta_0^{-3/5} n_{R_0,-1.5}^{3/5} \text{ Hz}. \end{aligned} \quad (50)$$

The highest frequency of the synchrotron emitted photons is expected at

$$\nu_{\text{max}}^{\text{ob.}}(t^{\text{ob.}} > t_1^{\text{ob.}}) = 6.5 \times 10^{23} (1+z)^{-1} E_{53}^{1/8} (\tilde{t}_{\text{day}}^{\text{ob.}})^{-3/8} n_{R_0,-1.5}^{-1/8} \text{ Hz}. \quad (51)$$

The total number of radiating electrons at radius $r \gg R_1$ is approximated by $N(r) = (4/3)N_1[(r/R_0)^3 - 1] \approx (4/3)N_1(r/R_0)^3$; thus, the asymptotic value of the flux emitted at $\nu_m^{\text{ob.}}$ is given by

$$F_{\text{max}}(t^{\text{ob.}} > t_1^{\text{ob.}}) = 38.7 E_{53} \epsilon_{B,-2}^{1/2} d_{L,28}^{-2} n_{R_0,-1.5}^{1/2} \text{ mJy} \quad (52)$$

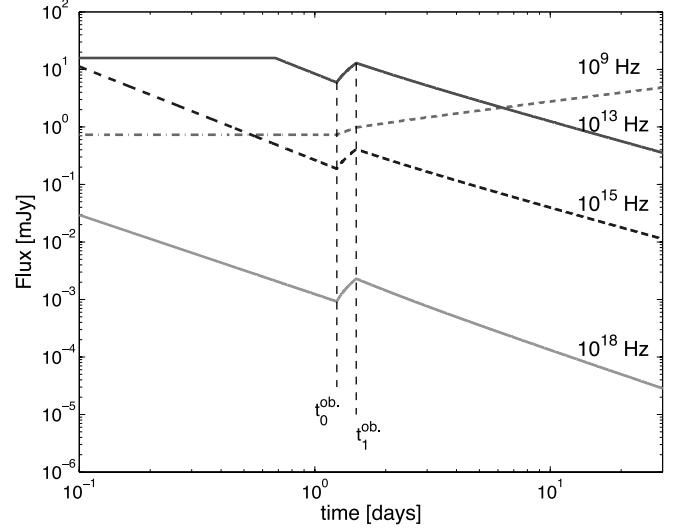


FIG. 4.—Schematic description of the light curves at different frequencies: radio (10^9 Hz), mid-IR (10^{13} Hz), optical (10^{15} Hz), and X-ray (10^{18} Hz). A power-law index $p = 2.5$ of the accelerated electrons and a luminosity distance $d_L = 10^{28}$ cm are assumed in producing this plot. [See the electronic edition of the Journal for a color version of this figure.]

(a somewhat lower value is expected at $r \gtrsim R_1$, with no simple dependence on the values of the unknown parameters).

5.4. Predicted Afterglow Light Curves

Light curves are calculated using standard formulae for the flux at a given frequency (e.g., Sari et al. 1998),

$$F_\nu = \begin{cases} F_{\text{max}}(\nu_{\text{ssa}}/\nu_m)^{1/3}(\nu/\nu_{\text{ssa}})^2, & \nu < \nu_{\text{ssa}}, \\ F_{\text{max}}(\nu/\nu_m)^{1/3}, & \nu_{\text{ssa}} < \nu < \nu_m, \\ F_{\text{max}}(\nu/\nu_m)^{-(p-1)/2}, & \nu_m < \nu < \nu_c, \\ F_{\text{max}}(\nu_c/\nu_m)^{-(p-1)/2}(\nu/\nu_c)^{-p/2}, & \nu_c < \nu < \nu_{\text{max}}. \end{cases} \quad (53)$$

The calculation is done separately for each of the three different phases. In the intermediate phase $t_0^{\text{ob.}} < t^{\text{ob.}} < t_1^{\text{ob.}}$, emission from the three different emitting regions is calculated separately and summed up.

The resulting light curves for radio (10^9 Hz), mid-infrared (mid-IR; 10^{13} Hz), optical (10^{15} Hz), and X-ray (10^{18} Hz) frequencies are presented in Figure 4. In producing this figure, characteristic values of $R_{0,18} = 1.6$, $n_{R_0,-1.5} = 0.4$ were assumed, which result in $t_0^{\text{ob.}} \approx 0.6$ days and $\Delta t^{\text{ob.}} = 0.13$ days (see eqs. [3], [4], [19], and [26]). The radio band is at the characteristic frequency of the synchrotron self-absorption frequency at all times, the mid-IR frequency is close to the peak emission, the optical band is typically higher than $\nu_m^{\text{ob.}}$ and lower than $\nu_c^{\text{ob.}}$, and the X-ray frequency is above $\nu_c^{\text{ob.}}$ for the characteristic parameters chosen.

Two important features of this scenario are seen in this figure. The first, which is common to all frequencies, is the increase of the flux by a factor of $\gtrsim 2$ from $t_0^{\text{ob.}}$ to $t_1^{\text{ob.}}$ caused by the simultaneous radiation from the three different regions during this period. The second feature is the flattening of the power-law index α of the flux time dependence [$F_\nu \propto t^{-\alpha}$, where $\alpha = \alpha(\nu)$ is frequency dependent] from its value at $t^{\text{ob.}} < t_0^{\text{ob.}}$ to a value smaller by $\frac{1}{2}$ at late times, $t^{\text{ob.}} > t_1^{\text{ob.}}$. This flattening is caused by

the change of the ambient density profile from $n(r) \propto r^{-2}$ at $t_0^{\text{ob.}} < t_0^{\text{ob.}}$ to a constant-density profile, $n(r) \propto r^0$ at late times of the blast wave evolution. The power-law index therefore changes accordingly: for $\nu < \nu_{\text{ssa}}$, $F_\nu \propto t^1$ if $n(r) \propto r^{-2}$, and $F_\nu \propto t^{1/2}$ if $n(r) \propto r^0$; for $\nu_{\text{ssa}} < \nu < \nu_m$, $F_\nu \propto t^0$ if $n(r) \propto r^{-2}$, and $F_\nu \propto t^{-1/2}$ if $n(r) \propto r^0$; and for $\nu_m < \nu < \nu_c$, $F_\nu \propto t^{-(3p-1)/4}$ if $n(r) \propto r^{-2}$, and $F_\nu \propto t^{-(3p-3)/4}$ if $n(r) \propto r^0$. At high frequencies, the light-curve time dependence is not changed by the change of the density profile, $F_\nu \propto t^{-(3p-2)/4}$ for $\nu > \nu_c$.

6. SUMMARY AND DISCUSSION

In this work, we considered the scenario of a massive star as a GRB progenitor. This scenario results in a complex structure of the circumburst medium, which is composed of four different regions: unshocked wind, shocked wind, shocked ISM, and unshocked ISM. We showed that the main effect takes place when the blast wave reaches the wind reverse shock, which separates the unshocked wind and the shocked wind regions. The blast wave then splits, and a blast wave reverse shock is formed. We showed in § 3 that the blast wave reverse shock, which separates two hot regions is not strong. By solving the equations describing the shock jump conditions, we showed that as long as the reverse shock exists, the shocked plasma moves at constant velocity, and a simple analytic relation between the Lorentz factors of the flow at the different regimes exists (eq. [11]). We then calculated the blast wave evolution and the resulting light curves at different frequencies (§ 5, Fig. 4).

The resulting light curves are significantly different than “standard” afterglow light curves calculations, which assume explosion into a uniform medium, or into a density gradient. The resulting light curve in the scenario presented here is similar to the light curve of an explosion into a density gradient at early times before the flux rise and to light curves obtained for an explosion into a uniform medium at late times. It has an important additional feature: during a short transition, lasting $\Delta t^{\text{ob.}}/t_0^{\text{ob.}} \simeq \frac{1}{5}$ of the transition time, which is expected to take place at $\simeq 1$ day after the GRB explosion, the flux rises by a factor of $\gtrsim 2$ at all frequencies. Such a rise in the flux is a prediction of this model. This model may therefore provide a natural explanation to the

rise in the various optical-band fluxes of GRB 030329 by a factor of 4 observed after ~ 1.4 days (Lipkin et al. 2004).

The occurrence time of the transition $t_0^{\text{ob.}}$ is the time at which radiation that was emitted as the blast wave reached the radius of the wind reverse shock R_0 is observed. This time is weakly constrained, being strongly dependent on the unknown values of R_0 and of the wind density at this radius, n_{R_0} . Therefore, characteristic transition occurrence times lasting between a few hours to several days may be expected. The transition time $\Delta t^{\text{ob.}}$, on the other hand, has the same parametric dependence as $t_0^{\text{ob.}}$. We therefore expect longer rise of the flux in bursts for which the transition occurs at late times, compared to bursts for which the transition occurs at earlier times.

The purely constrained value of the transition time $t_0^{\text{ob.}}$ implies that observed afterglow light curves from different bursts may be interpreted as resulting from explosion into a uniform medium, or into a density gradient, if only part of the data is available. Thus, we find that both interpretations (e.g., Chevalier & Li 2000) may be consistent with the data, with preferably parameters that fit an explosion into a uniform medium at very late times.

We used here a highly simplified model to describe the density profile of the ambient matter. We did not consider radiative cooling, which is highly uncertain, and, if it exists, lowers the temperature of the shocked wind gas in region (b), hence increasing its density. We also did not consider inhomogeneities inside the different regions, which may also have observational consequences. The calculation presented in § 3 for the interaction of a relativistic blast wave with a density discontinuity caused by a strong shock is, however, general and can be used in the context of supernovae calculations as well. We thus conclude that the main findings of this work—the afterglow rebrightening by a factor of $\gtrsim 2$ and the different light curves slopes at early and late times—remain valid also in a more complex and realistic ambient medium profile.

A. P. wishes to thank James Miller-Jones and Peter Mészáros for useful discussions. This research was supported by NWO grant 639.043.302 to R. W. and by the EU under RTN grant HPRN-CT-2002-00294.

APPENDIX

RELATION BETWEEN THE OBSERVED TIME AND EMISSION RADIUS IN A RELATIVISTIC FIREBALL

Waxman (1997) calculated the relation between the observed time delay $\Delta t^{\text{ob.}}$ of photons emitted by synchrotron radiation from a shell expanding relativistically and self-similarly in a uniform medium as the shell's front reaches radius r , with respect to photons emitted from the center of the explosion at $r = 0$, and found the relation $\Delta t^{\text{ob.}} \simeq r/[4\Gamma^2(r)c]$. Here, we repeat the calculation for the case of a relativistic expansion in a density gradient, $n(r) \propto r^{-p}$. In this case, assuming adiabatic expansion, the Lorentz factor of the flow scales with the radius as $\Gamma(r) \propto r^{-(3-p)/2}$. The magnetic field scales as $B \propto \Gamma(r)n(r)^{1/2} \propto r^{-3/2}$, and the characteristic Lorentz factor of the electrons scales as $\gamma_{\text{char}} \propto \Gamma(r)$. The peak frequency of the synchrotron emitted photons (in the comoving frame) therefore scales as $\nu_m \propto \gamma_{\text{char}}^2 B \propto r^{p-9/2}$.

The number of photons emitted by a single electron at a unit comoving time \dot{N}_γ is proportional to the magnetic field B . The total number of electrons swept up by the shell (and, presumably, emit) at radius r is $N_e(r) \propto r^{3-p}$. Since the comoving time during which the plasma propagates a distance dr is $dt^{\text{co.}} \simeq dr/\Gamma(r)c$, the number of photons emitted as the plasma expands a distance dr scales as $dN_\gamma/dr \propto N_e N_\gamma (dt^{\text{co.}}/dr) \propto r^{3-3p/2}$. The fraction of photons emitted at frequency ν_m that are observed at frequency $\nu_m^{\text{ob.}}$ is given by equation (5) of Waxman (1997), $df/d\nu_m^{\text{ob.}} \simeq (2\Gamma\nu_m)^{-1}$, where $\Gamma \gg 1$ assumed. Thus, the number of photons produced by the fireball shell at radius r with frequency in the range $\nu_m^{\text{ob.}} \dots \nu_m^{\text{ob.}} + d\nu_m^{\text{ob.}}$ is

$$\frac{d^2 N_\gamma}{d\nu_m^{\text{ob.}} dr} \propto \frac{dN_\gamma}{dr} \Gamma(r)^{-1} \nu_m^{-1} \propto r^{3(3-p)}. \quad (\text{A1})$$

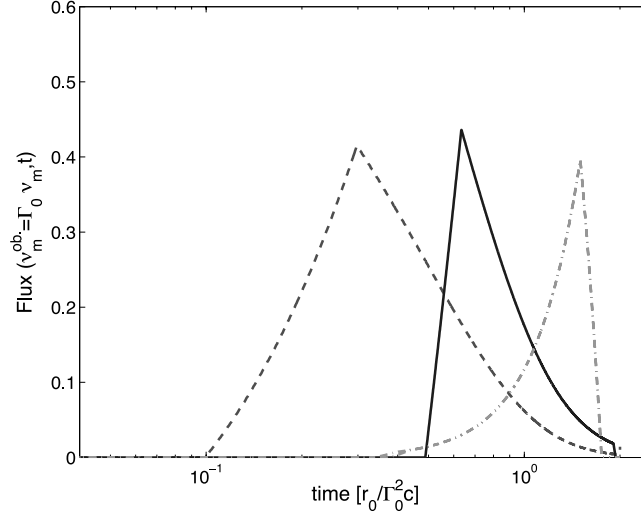


FIG. 5.—Normalized observed flux at observed frequency ν_m as a function of time, for various considered density profiles. The solid line shows the result for a density profile $n(r) \propto r^{-2}$, as expected in the early stages of the blast wave evolution, at $r < R_0$. The dashed line presents the results for an expansion in a homogeneous medium and is similar to the results of Waxman (1997). The dash-dotted line represents a scenario of an r -independent Lorentz factor and magnetic field, as expected for $R_0 < r < R_1$. [See the electronic edition of the Journal for a color version of this figure.]

The delay in observed time of a photon emitted from the edge of the shell at frequency ν_m and observed at frequency ν_m^{ob} , with respect to photons emitted on the line of sight is given by (for $\Gamma \gg 1$)

$$\Delta t_\theta(\nu_m^{\text{ob}}, r) = \frac{r}{\Gamma^2 c} \left(\Gamma \frac{\nu_m}{\nu_m^{\text{ob}}} - \frac{1}{2} \right) \propto r^{4-p} \left(r^{-6+3p/2} - \frac{1}{2} \right). \quad (\text{A2})$$

An additional delay exists between photons emitted at radius r on the line of sight, compared to photons emitted from the center of the explosion at $r = 0$,

$$\Delta t_r(r) = \frac{r}{c} - \int_0^r \frac{dr}{[1 - 1/2\Gamma^2(r)]^{1/2} c} = \frac{r}{4(4-p)\Gamma^2(r)c}. \quad (\text{A3})$$

Assuming that photons are emitted uniformly from a shell of finite thickness $\xi r/\Gamma^2 c$, the arrival time of photons emitted at radius r and observed with frequency ν_m^{ob} are uniformly distributed over the range $t(\nu_m^{\text{ob}}, r) = \Delta t_\theta(\nu_m^{\text{ob}}, r) + \Delta t_r(r)$ to $t(\nu_m^{\text{ob}}, r) + \tau_\xi$, where $\tau_\xi = \xi r/\Gamma^2 c$.

Figure 5 shows the results of a numerical calculation of the flux as a function of time (compare with Fig. 1 of Waxman [1997]). The width of the shell considered is $\xi = \frac{1}{8}$. The three plots represent the three cases considered in this work. Explosion into a density gradient, $n(r) \propto r^{-2}$, is presented by the solid curve, and explosion into a uniform medium is presented by the dashed curve. The dash-dotted curve represents the special scenario that exists in the intermediate phase of the blast wave evolution at $R_0 < r < R_1$, during which the Lorentz factor and the magnetic field are kept constant as long as the reverse shock exists.

We thus conclude that while for an expansion into uniform medium, the Waxman (1997) relation, $t^{\text{ob}} \simeq r/4\Gamma^2 c$ holds, for an explosion into density gradient, $n(r) \propto r^{-2}$ this relation is modified and is $t^{\text{ob}} \simeq r/2\Gamma^2 c$; while in the intermediate phase of the blast wave evolution, the correct relation is $t^{\text{ob}} \simeq r/\Gamma^2 c$.

REFERENCES

- Blandford, R. D., & McKee, C. F. 1976, *Phys. Fluids*, 19, 1130
 Castor, J., McCray, R., & Weaver, R. 1975, *ApJ*, 200, L107
 Chevalier, R. A., & Li, Z.-Y. 2000, *ApJ*, 536, 195
 Chevalier, R. A., Li, Z.-Y., & Fransson, C. 2004, *ApJ*, 606, 369
 Chieffi, A., et al. 2003, *MNRAS*, 345, 111
 Dyson, J. E., & Williams, D. A. 1997, *The Physics of the Interstellar Medium* (Bristol: IoP)
 Eldridge, J. J., Genet, F., Daigne, F., & Mochkovitch, R. 2006, *MNRAS*, 367, 186
 Fruchter, A. S., et al. 1999, *ApJ*, 519, L13
 Fynbo, J. P. U., et al. 2003, *A&A*, 406, L63
 Galama, T., & Wijers, R. A. M. J. 2001, *ApJ*, 549, L209
 Galama, T., et al. 1998, *Nature*, 395, 670
 García-Segura, G., & Franco, J. 1996, *ApJ*, 469, 171
 García-Segura, G., Langer, N., & Mac Low, M.-M. 1996a, *A&A*, 316, 133
 García-Segura, G., Mac Low, M.-M., & Langer, N. 1996b, *A&A*, 305, 229
 Garnavich, P. M., et al. 2003, *ApJ*, 582, 924
 Hjorth, J., et al. 2003, *Nature*, 423, 847
 Kouveliotou, C., et al. 1993, *ApJ*, 413, L101
 Landau, L. D., & Lifschitz, E. M. 1959, *Fluid Mechanics* (Reading: Addison-Wesley)
 Le Floch, E., et al. 2003, *A&A*, 400, 499
 Levinson, A., & Eichler, D. 1993, *ApJ*, 418, 386
 Lipkin, Y. M., et al. 2004, *ApJ*, 606, 381
 MacFadyen, A. I., & Woosley, S. E. 1999, *ApJ*, 524, 262
 MacFadyen, A. I., Woosley, S. E., & Heger, A. 2001, *ApJ*, 550, 410
 Malesani, D., et al. 2004, *ApJ*, 609, L5
 Paczyński, B. 1998, *ApJ*, 494, L45
 Petrovic, J., Langer, N., Yoon, S.-C., & Heger, A. 2005, *A&A*, 435, 247
 Ramirez-Ruiz, E., Dray, L. M., Madau, P., & Tout, C. A. 2001, *MNRAS*, 327, 829
 Ramirez-Ruiz, E., García-Segura, G., Salmonson, J. D., & Pérez-Rendón, B. 2005, *ApJ*, 631, 435
 Sari, R., & Piran, T. 1995, *ApJ*, 455, L143
 Sari, R., Piran, T., & Narayan, R. 1998, *ApJ*, 497, L17
 Stanek, K. Z., et al. 2003, *ApJ*, 591, L17

- Trentham, N., Ramirez-Ruiz, E., & Blain, A. W. 2002, MNRAS, 334, 983
van Paradijs, J., Kouveliotou, C., & Wijers, R. A. M. J. 2000, ARA&A, 38, 379
Vink, J. S., & de Koter, A. 2005, A&A, 442, 587
Vink, J. S., de Koter, A., & Lamers, H. J. G. L. M. 2000, A&A, 362, 295
Vreeswijk, P. M., et al. 2004, A&A, 419, 927
Waxman, E. 1997, ApJ, 491, L19
Weaver, R., McCray, R., Castor, J., Shapiro, P., & Moore, M. 1977, ApJ, 218, 377
Wijers, R. A. M. J. 2001, in Gamma Ray Bursts in the Afterglow Era, ed. E. Costa, F. Frontera, & J. Hjorth (Berlin: Springer), 306
Wijers, R. A. M. J., & Galama, T. J. 1999, ApJ, 523, 177
Wijers, R. A. M. J., Rees, M. J., & Mészáros, M. 1997, MNRAS, 288, L51
Wijers, R. A. M. J., et al. 1998, MNRAS, 294, L13
Woosley, S. E. 1993, ApJ, 405, 273
Zhang, W., Woosley, S. E., & MacFadyen, A. I. 2003, ApJ, 586, 356